CHINA FOUNDRY Research & Development
Vol.13 No. 6 November 2016
DOI: 10.1007/s41230-016-6044-4

Numerical simulation on vacuum solution heat treatment and gas quenching process of a low rhenium-containing Ni-based single crystal turbine blade

Zhe-xin Xu, Xiang-lin Su, *Qing-yan Xu, and Bai-cheng Liu

Key Laboratory for Advanced Materials Processing Technology (Ministry of Education), School of Materials Science and Engineering, Tsinghua University, Beijing 100084, China

Abstract: Numerical heat-transfer and turbulent flow model for an industrial high-pressure gas quenching vacuum furnace was established to simulate the heating, holding and gas fan quenching of a low rhenium-bearing Ni-based single crystal turbine blade. The mesh of simplified furnace model was built using finite volume method and the boundary conditions were set up according to the practical process. Simulation results show that the turbine blade geometry and the mutual shielding among blades have significant influence on the uniformity of the temperature distribution. The temperature distribution at sharp corner, thin wall and corner part is higher than that at thick wall part of blade during heating, and the isotherms show a toroidal line to the center of thick wall. The temperature of sheltered units is lower than that of the remaining part of blade. When there is no shelteration among multiple blades, the temperature distribution for all blades is almost identical. The fluid velocity field, temperature field and cooling curves of the single and multiple turbine blades during gas fan quenching were also simulated. Modeling results indicate that the loading tray, free outlet and the location of turbine blades have important influences on the flow field. The high-speed gas flows out from the nozzle is divided by loading tray, and the free outlet enhanced the two vortex flow at the end of the furnace door. The closer the blade is to the exhaust outlet and the nozzle, the greater the flow velocity is and the more adequate the flow is. The blade geometry has an effect on the cooling for single blade and multiple blades during gas fan quenching, and the effects in double layers differs from that in single layer. For single blade, the cooing rate at thin-walled part is lower than that at thick-walled part, the cooling rate at sharp corner is greater than that at tenon and blade platform, and the temperature at regions close to the internal position is decreased more slowly than that close to the surface. For multiple blades in single layer, the temperature at sharp corner or thin wall in the blade that close to the nozzles is much lower, and the temperature distribution of blades is almost parallel. The cooling rate inside the air current channel is lower than that of at the position near blade platform and tenon, and the effect of blade location to the nozzles on the temperature field inside the blade is lower than that on the blade surface. For multiple blades in double layers, the flow velocity is low, and the flow is not uniform for blades in the second-layer due to the shielding of blades in the first-layer. the cooling rate of blades in the second-layer is lower than that in the first-layer. The cooling rate of blade close to the nozzles in the first-layer is the higher than that of blade away from the nozzles in the second-layer, and the temperature distribution on blades in the same layer is almost parallel. The cooling rate in thin wall position of blade away from the nozzles is larger than that in tenon of the blade closer to the nozzles in the same layer. The cooling rate for blades in the second-layer is much lower both in thin wall and tenon for blades away from the nozzles.

Key words: Ni-based superalloy; incipient melting; cooling rates; turbine blade

CLC numbers: TP391.9 **Document code:** A **Article ID:** 1672-6421(2016)06-402-12

***Qing-yan Xu**

Male, born in 1971, Ph.D, professor. His current research mainly focuses on a wide range of topics within the field of mechanical engineering, manufacturing process, materials engineering and integrated computational materials engineering. He is an author/co-author of over 100 peer-reviewed journals/ conference papers, 5 edited books and 6 patents.

E-mail:scjxqy@tsinghua.edu.cn

Received: 2016-04-28; Accepted: 2016-07-25

Turbine blades are subjected to extremely severe service environment inside a gas turbine engine, including high working temperature, high pressure, high speed rotation, complex working stress, and gas corrosion and erosion conditions. This could result in blade failures, which can cripple the engine performance. The turbine blades therefore must be carefully designed and manufactured to withstand the strenuous environment [1-4]. Ni-based superalloys are the optimum materials used for fabricating turbine

blades of aircraft engines and industrial gas turbines due to their excellent tensile properties, creep rupture, and fatigue properties, superior resistance to oxidation and hot corrosion, and good microstructure stability at high temperatures [1-5]. To achieve the required high temperature properites, especially high creep strength of turbine blades, Ni-based superalloys were developed from conventional casting alloys to single crystal alloys characterized by adding increasing amounts of dense refractory elements such as Re and Ru [6-11], and the turbine blades were evolved from conventionally solidified equiaxed-grained blades to directionally solidified columnar-grained and single crystal blades [1-3, 5, 12-13].

During the investment casting process of single crystal turbine blades, primary γ dendrite solidification is accompanied by solute partitioning at solid-liquid interface [14-16]. Some solute elements segregate to the dendrite core, while other solute elements segregate to the interdendritic liquid, which leads to the formation of non-equilibrium interdendritic constituents, including the coarse, irregular shaped and incoherent γ' precipitates and a high volume fraction of coarse eutectic γ/γ', resulting in severe chemical segregation across the microstructure of single crystal turbine blades [14-16]. The interdendritic coarse γ' precipitates, incoherent γ-γ' interface, undissolved eutectics γ/γ', severe chemical segregation is detrimental to the strength, creep rupture resistance and fatigue properties of single crystal turbine blades [14-21]. Consequently, the as-cast single crystal turbine blades must be solution heat treated to dissolve eutectic γ/γ', minimize chemical segregation, and solutionize the coarse γ' precipitates for reprecipitation during subsequent ageing heat treatments to confer the mechanical properties at high temperatures. To minimize the incipient melting resulted from the highly segregated as-cast microstructure, stepwise solution heat treatment schemes are utilized to homogenize the single crystal turbine blades. The single crystal turbine blades are solutionized under Ar atmosphere in a vacuum heat treatment furnace and rapidly gas fan quenched using high purity forced argon flow giving an appropriate cooling rate at the final soak cycle. According to the change of temperature field, the solution heat treatment is composed of vacuum heating, holding, and gas fan quenching process. Due to the poor thermal conductivity and complex structure of single crystal turbine blade components, precise control of the thermal history during processing is needed to avoid incipient melting and to develop optimized mechanical properties for service applications.

Trial-and-error procedures are adopted to optimize the processing conditions for the heat treatment of single crystal turbine blades and considerable reliance is placed on empiricism and practical experience. However, with the rapid advances in computing hardware and software, computational fluid dynamics (CFD) has become an effective tool for studying the heat-transfer and fluid flow problems. It allows to investigate the effect of individual factor without changing other experimental parameters and provides reliable modeling results for optimizing practical processing conditions. Patankar and Spalding [22] presented furnace simulations to model fluid flow and heat transfer in three-dimensional furnaces and qualitative predictions show good agreements with experimental validations. Kang and Rong [23] proposed a hybrid method of analytical equation and numerical calculations using empirical correlations for natural and forced convection. Li et al. [24] researched the effect of heat transfer coefficient, the preheat temperature and the quenching temperature on residual stress, hardness, distortion and other quenching results in the process of high pressure gas quenching. Morsi Y, et al. [25] adopted a transient flow model and Wang et al. [26] established the flow and heat-transfer model to simulate the high pressure gas quenching process of a large H13 die based on the CFD package, respectively. Numerical simulation has been carried out by Francesco Cosentino et al.[27-29] to predict the temporal evolution of temperature distribution inside the treated component, to calculate heat transfer coefficients, to analyze the homogeneity of heat transfer, and to model the flow field in the furnace during heat treatment of single crystal Ni-based superalloys. Much previous work focused on the high pressure gas quenching process of die steel. Although gas fan quenching process simulation with CFD has been investigated for vacuum heat treatment of single crystal Ni-based superalloys[27-29], the results have considerable discrepancy for industrial production practice. They subdivided the laboratory scale vacuum furnace in three separated models, which run individually and are coupled by transferring boundary conditions, and the effective thermal conductivity are neglected in simulation. The temperature distribution for the components is ignored. These simplifications and approximations may bring out errors and discrepancies for practical vacuum heat treatment of single crystal Ni-based superalloys.

DD6 alloy is a low cost second generation single crystal Ni-based superalloy, which contains lower rhenium, possesses superior tensile properties, creep rupture properties, oxidation resistance and hot corrosion resistance compared with its counterparts PWA1484, CMSX-4, SC180, and René N5 [30-31], and can be utilized to manufacture the turbine blades for aero-engines and industrial gas turbine engines. However, numerical modeling for the vacuum solution heat treatment and gas fan quenching process of DD6 turbine blade is rarely reported in literature. The objective of present research is therefore to systematically investigate the vacuum solution heat treatment and gas quenching process of DD6 turbine blade. The numerical heat-transfer and turbulent flow model based on the CFD software package and the practical 3D-reconstruction of an industrial high-pressure quenching vacuum heat-treatment furnace is established to simulate the heating, holding and gas fan quenching process of DD6 turbine blades.

1 Set-up of vacuum furnace chamber

The high pressure gas fan quenching vacuum heat treatment furnace used was manufactured by Beijing Huaxiang Vacuum Heat Treatment Equipment Co. Ltd. with the model of HZQ-100. The cylindrical chamber of vacuum furnace and its geometry are shown in Fig. 1(a) and (b), respectively. The working dimensions of the

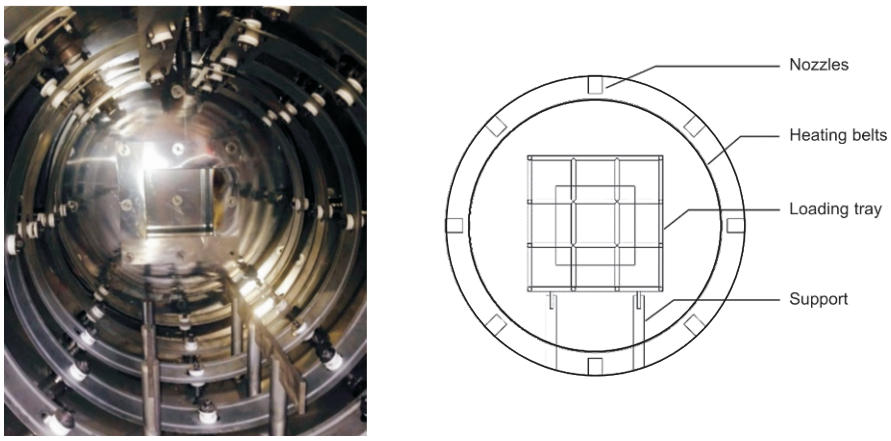

(a) Cylindrical chamber of vacuum furnace (b) Geometry of the furnace chamber

Fig. 1: Cylindrical chamber of high pressure gas fan quenching vacuum furnace (a) and corresponding geometry of furnace chamber (b)

furnace are 300 mm × 300 mm × 400 mm with a recommended load of up to 80 kg and a loading tray made of refractory steel. Gas enters the chamber from circumferential nozzles and the hot gas leaves the heating chamber through outlet. The gas is recycled in a continuous gas quenching process when the hot gas flows through the heat exchanger and cools down.

The free outlet structure in the furnace chamber is shown in Fig. 2. The free outlet is a square outlet of 180 mm × 180 mm, which is connected to the circulating air tube of the vacuum furnace. The effect of the free outlet structure on the flow field is also considered.

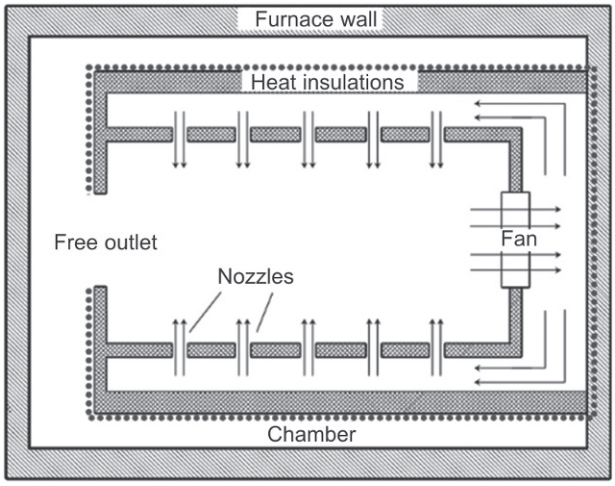

Fig. 2: Schematic illustration of free-outlet chamber structure

The solution heat treatment including heating, holding and gas fan quenching was performed according to the standard solution heat treatment schedules of DD6 alloy, as shown in Fig. 3. The temperature program was heating at 3 ºC•min^{-1} from room temperature to 1,290 °C. The turbine blade was heat treated at 1,290 °C for 1 h, 1,300 °C for 2 h, and 1,315 °C for 4 h. At the final stage of solution heat treatment, the turbine blades were immediately gas furnace quenched using high purity forced high pressure argon flow with a cooling rate larger than 300 °C•min^{-1}.

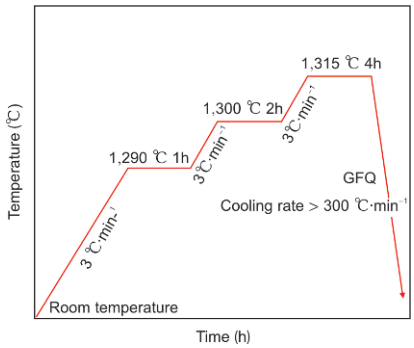

Fig. 3: Schematic illustration of standard solution heat treatment schedules for DD6 alloy

2 Formulation of vacuum solution heat treatment process

2.1 Transport equations in heating and holding stage

In the heating stage, the heat transfer mode in furnace chamber is heat radiation and heat conduction. It is assumed that the radiative heat transfer occurs at a vacuum condition and therefore the surface-to-surface (S2S) method is applied to simulate the radiative heat transfer. The radiation depends only on the surface of the heat transfer, and the medium heat transfer is ignored. The object of radiation heat transfer is considered to be all gray body, and the reflection is seen as a diffuse reflection. The reflection between two surfaces meets the formula as:

$$\frac{Q_2}{A_2} = F_{21}\sigma\varepsilon_2(T_2^4 - T_1^4) \quad (1)$$

where Q_2 is the net heat flux, A_2 is the area of the radiative surface, σ is the Stefan-Boltzmann constant, ε_2 is the emissivity of the radiative surface, T_1 is the temperature of radiative surface 1, T_2 is the temperature of radiative surface 2, F_{21} is the view factor between the two surfaces and defined by

$$F_{21} = \frac{1}{\pi A_2}\int dA_2 \int_{\Omega} \frac{cos(\theta_1)cos(\theta_2)dA_2}{l_{21}^2} \quad (2)$$

where θ_1 and θ_2 represents the angle between the surface normal

and a ray between the two differential areas, respectively. l_{21} is the distance between two surfaces.

The radiation exchange of the surfaces is described by

$$\sum_{j=1\,i\neq j}^{N}\left(F_{ij}\frac{1-\varepsilon_j}{\varepsilon_j}\right)\frac{Q_{ij}}{A_j}=\sum_{j=1\,i\neq j}^{N}F_{ij}\sigma\left(T_j^4-T_i^4\right) \quad (3)$$

where ε_j is the emissivity of surface j.

The transport of energy for the solid is described by

$$\frac{\partial\rho H}{\partial t}-\nabla\cdot(\lambda\nabla T)=S_h \quad (4)$$

where ρ is the mean fluid density, H is the total enthalpy, λ is the thermal conductivity, T is the temperature, S_h is the source term.

2.2 Transport equations during gas fan quenching

Flow and heat transfer during cooling process are investigated using CFD model. Only the forced convection is considered. The buoyancy caused by the natural convection and density change is neglected. The heat transfer mode during the quenching process is convection heat transfer and heat conduction and the radiation heat transfer is neglected [32-33]. When the Reynolds number (R_e) is greater than the critical Reynolds number during gas fan quenching, the fluid flow treated as the turbulent flow. Turbulent flow model applies the two-equation κ-ε turbulence model. The governing equations for the continuity equation, momentum equation, energy equation, turbulence kinetic energy equation and turbulence dissipation rate equation are as follows:

Continuity equation

$$\frac{\partial\rho}{\partial t}+\nabla\cdot(\rho U)=0 \quad (5)$$

where ρ is the mean fluid density and U is the velocity, t is the time.

Momentum equation

$$\frac{\partial\rho U}{\partial t}+\nabla\cdot(\rho U\times U)-\nabla\cdot\left(\mu_{eff}\nabla U\right)=-\nabla p+\nabla\cdot\left(\mu_{eff}(\nabla U)^T\right)+\mathrm{B} \quad (6)$$

where B is the body force, p is the pressure, and μ_{eff} represents the effective viscosity:

$$\mu_{eff}=\mu+\mu_T \quad (7)$$

where μ and μ_T are laminar viscosity and turbulent viscosity:

$$\mu=\frac{\rho V_\infty l}{Re}\quad \mu_T=C_\mu\rho\frac{\mathrm{k}^2}{\varepsilon} \quad (8)$$

where Re is the Reynolds number, V_∞ is the fluid velocity, l is characteristic length, μ is solved by using definition of Reynolds number. μ_T is solved by using κ-ε turbulence model, in which k represents turbulence kinetic energy, and ε represents turbulence dissipation rate. C_μ is a model constant giving in Table 1.

Energy equation for the fluid

$$\frac{\partial\rho H}{\partial t}+\nabla\cdot(\rho UH)-\nabla\cdot(\lambda\nabla T)=S_h \quad (9)$$

where H is the total enthalpy, t is time, λ is the thermal conductivity, T is the temperature, S_h is the source term.

Energy equation for the solid is given in Eq. (4).

Turbulence kinetic energy equation

$$\frac{\partial\rho k}{\partial t}+\nabla\cdot(\rho Uk)-\nabla\cdot\left(\left(\mu+\frac{\mu_T}{\sigma_k}\right)\nabla k\right)=G_k-\rho\varepsilon \quad (10)$$

where σ_k is a model constant given in Table 1. G_k is the generation of turbulence kinetic energy (as known as k) due to the mean velocity gradients, and defined by

$$G_k=\mu_T\nabla U\cdot(\nabla U+(\nabla U)^T)-\frac{2}{3}\nabla\cdot U(\mu_T\nabla\cdot U+\rho k) \quad (11)$$

Turbulence dissipation rate equation

$$\frac{\partial\rho\varepsilon}{\partial t}+\nabla\cdot(\rho U\varepsilon)-\nabla\cdot\left(\left(\mu+\frac{\mu_T}{\sigma_\varepsilon}\right)\nabla\varepsilon\right)=\frac{\varepsilon}{k}(C_1G_k-C_2\rho\varepsilon) \quad (12)$$

where C_1 and C_2 are model constants given in Table 1.

Table 1: Constants used for *k*-ε model calculation

C_μ	C_1	C_2	σ_k	σ_ε
0.09	1.44	1.92	1.0	1.3

2.3 Boundary and initial conditions

In the model of ramping-up stage, the initial heating temperature is room temperature. The heating source is simplified on annular heating belts and the temperature boundary condition of the heating belt is calculated by User Defined Function (UDF) method in Fluent V13 ANSYS. It is considered that the temperature of heating belts is homogeneous. The condition of the chamber walls is considered to be adiabatic condition as the walls are molybdenum metal heat insulations. In the model of quenching stage, it is assumed that the furnace walls are adiabatic, no slip condition is adopted in the wall surfaces, and during the quenching process, the gas velocity entering the furnace chamber through every nozzle is a constant. The gas is argon, and the operating pressure is constant from 3 bar to 9 bar. It is considered that the components temperature is homogeneous, and the initial quenching temperature of loading tray is 1,315 °C. The velocity, temperature, pressure, turbulent kinetic energy, and turbulent dissipation rate of inlet gas are uniformly distributed on the inlet cross section, and the same inlet conditions of all nozzles are set.

2.4 Material properties

In simulation, for the argon gas, the ideal incompressible model was used, which means the density of argon is constant during computation. The thermal conductivity and heat capacity of DD6 alloy are defined as piecewise-linear function of the temperature from room temperature to 1,315 °C, which is given in Table 2. The loading tray is considered to be conduction solid with physical properties of refractory steel.

2.5 Finite volume method modeling

The commercial CFD software package Fluent V13 ANSYS was employed for the calculation and modeling. The mesh of the practical vacuum furnace chamber model is shown in Fig. 4. The amount of cells ranges from 900 thousand to 3.5 million depending on the number of loading blades. The numerical analysis was performed with a control volume approach, and all equations were solved using the second-order upwind discretization for convection and SIMPLE algorithm.

Table 2: Thermal conductivity and heat capacity of DD6 alloy [34]

Temp. (°C)	100	200	300	400	500	600	700	800	900	1000	1100	1200	1300
Thermal conductivity ($W•m^{-1}•°C^{-1}$)	8.00	9.45	11.15	13.4	15.35	17.60	20.20	22.30	24.55	26.80	28.95	30.90	33.20
Heat capacity ($J•g^{-1}•°C^{-1}$)	0.358	0.392	0.427	0.462	0.496	0.531	0.566	0.600	0.635	0.669	0.704	0.739	0.733

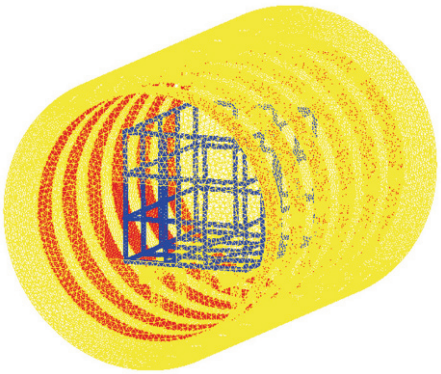

Fig. 4: Mesh of furnace chamber model

3 Results and discussion

3.1 Load-free experiment

A load-free heating experiment was conducted. Figure 5 shows the experimental condition and the thermocouple points in the loading tray.

Numerical simulations with different boundary conditions during no-load heating were carried out. Figure 6 shows the temperature curves at thermocouple points. Figure 6(a) shows the simulated and experimental temperature results at point 1, which indicates that the simulation result with UDF power input boundary condition is more approached to the experiment results. Figure 6(b) shows the simulated and experimental results of different points. The temperature difference between different points in loading tray gradually reduces, and the simulation results are close to the experiment results as the heating processes.

3.2 Temperature field prediction during heating and holding process

Figure 7 shows the temperature curves of surfaces on heating belts, turbine blade and a unit of loading tray during the heating process. In the initial stage of heating, different heated units have different thermal responses. According to radiative and heat transfer, the response rate of units to temperature variations depends on thermal physical properties of material, radiation shape factor and component structure in which those units are located at. Figure 8 demonstrates the temporal evolution of temperature distribution for single turbine blade during heating and holding stage. It indicates that the temperature of blade is higher than that of loading tray during initial heating and holding stage [Fig.8 (a) and (b)]. For the temperature field of a single turbine blade, the temperature uniformity during holding [Fig. 8(d) and (f)] stage is better than that during heating stage [Fig. 8(c) and (e)]. During heating, temperature distribution temperature distributions at the sharp corner and thin wall of single turbine blade are higher than that at the thick wall (such as tenon) of single blade [Fig. 8(c)]. The complex curved surface structure of turbine blade itself also have an effect on its heating process. Specifically, the temperature of sheltered units is lower than that of the air current channel within a blade and the complicated structure of tenon connection region of a turbine balde, even if the sheltered units in the thin wall [Fig. 8(e)].

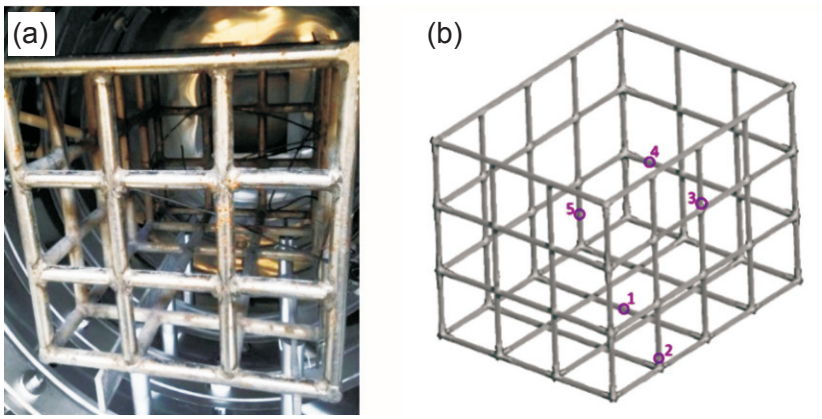

Fig. 5: Thermocouple arrangement (a) and position of thermocouple points (b)

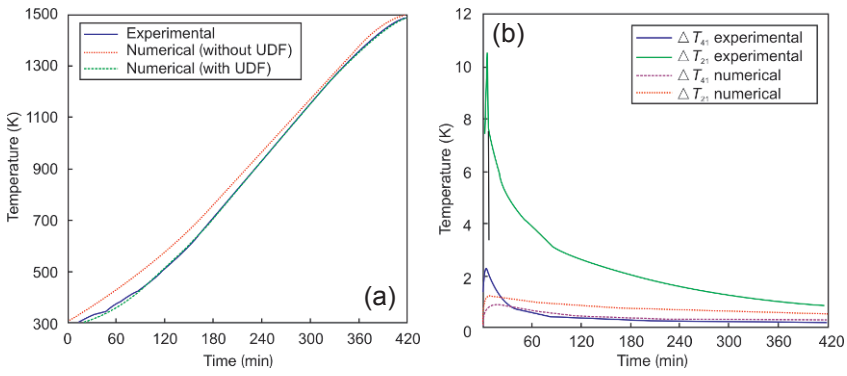

Fig. 6: Comparison of simulated (with UDF) and experimental temperature curves at different points in loading tray: (a) temperature curves in point 1; (b) temperature curves between point 1 and point 2 (ΔT_{21}), point 1 and point 4 (ΔT_{41})

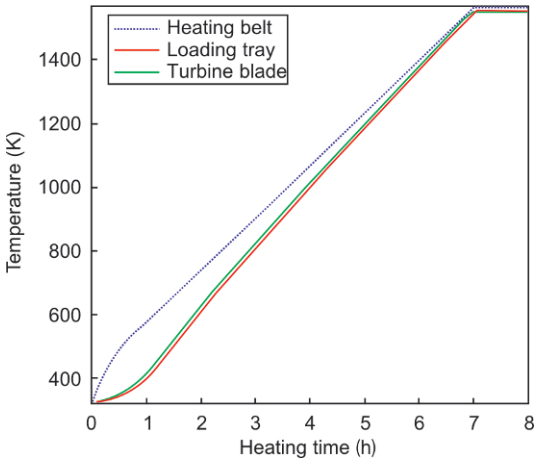

Fig. 7: Simulated temperature curves of surfaces on heating belts, turbine blade and loading tray during heating process

3.3 Effect of number of blades during heating and holding process

Figure 9 shows the loading pattern of multiple blades in one layer and double layers. The effect of multiple blades in single layer and double layers on temperature distribution during heating and holding is demonstrated in Fig.10 and Fig.11, respectively. The temperatn e field id strib ion of b ad s in a single layer is close to that they have not been sheltered [Fig. 10 (a)]. During heating and holding process, the temperature field uniformity does not change with alteration of the locating places due to the temperature difference among the multiple blades is smaller than that of a separate blade [Fig.10(a) and (b)]. The temperature distribution of multiple blades in double layers is homogeneous during heating and holding stages. There is no obvious shelteration among multiple blades with double layers and the temperature field distributions are almost identical for all blades [Fig. 11(a) and (b)].

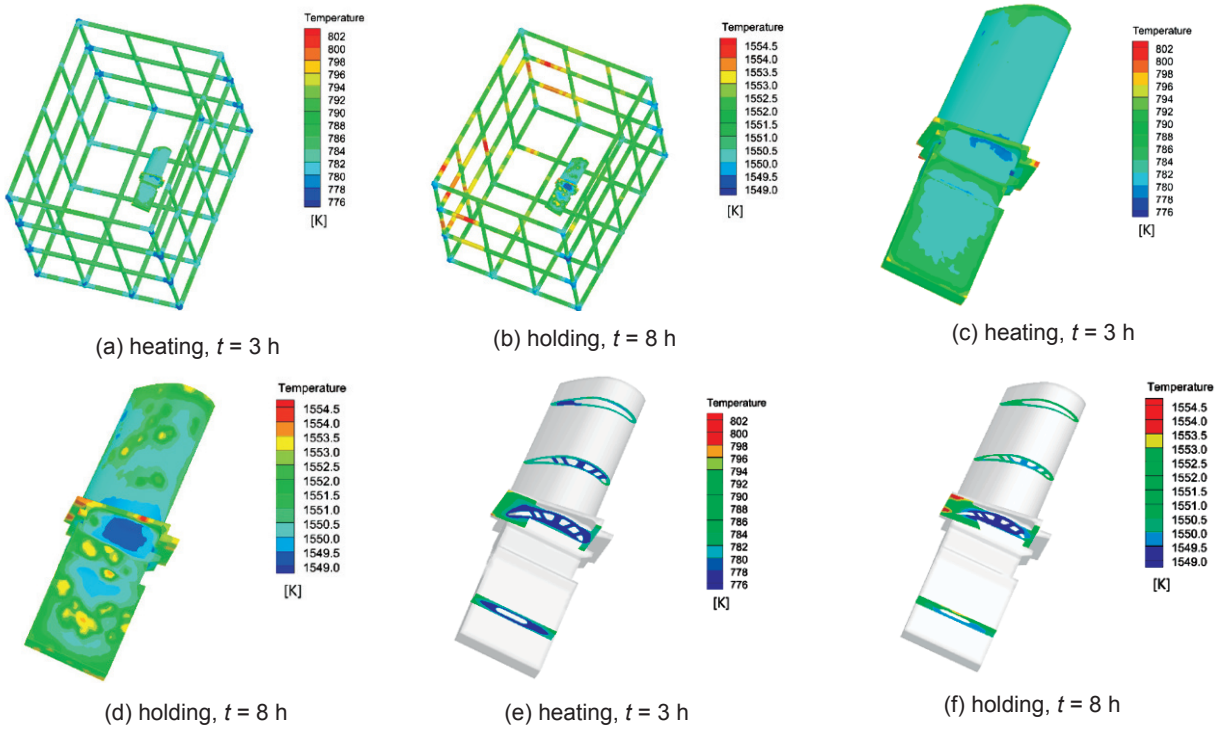

(a) heating, t = 3 h (b) holding, t = 8 h (c) heating, t = 3 h

(d) holding, t = 8 h (e) heating, t = 3 h (f) holding, t = 8 h

Fig. 8: Temperature distribution of single blade at different time during heating and holding stages in vacuum furnace: (a) and (b) temperature field in furnace; (c) and (d) temperature profiles on turbine blade surface; (e) and (f) temperature distribution in different sections of turbine blade

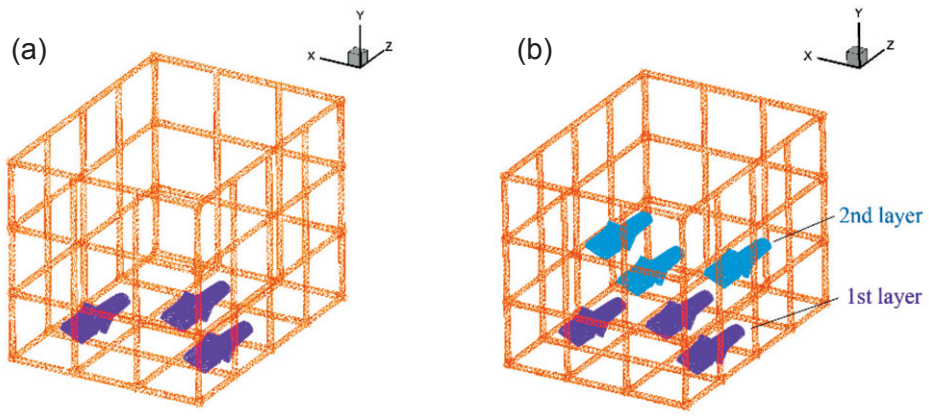

Fig. 9: Loading pattern of multiple blades in a single layer (a) and double layers (b)

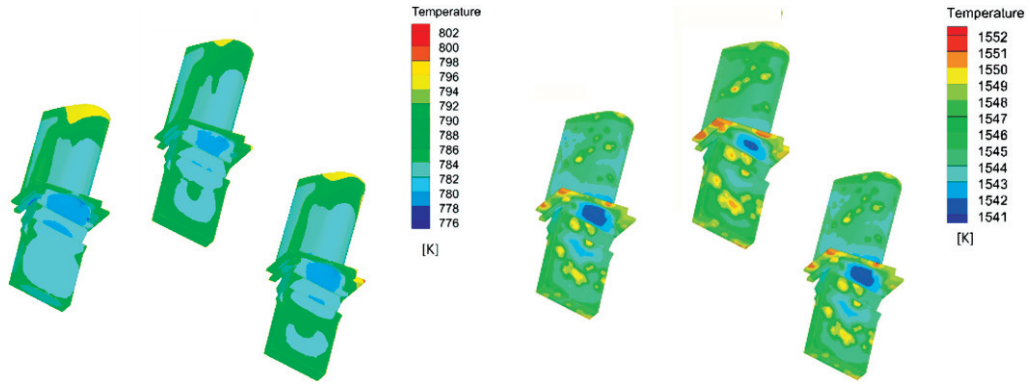

(a) heating, t = 3 h (b) holding, t = 8 h

Fig. 10: Temperature distribution of multiple blades with one layer during heating and holding stages

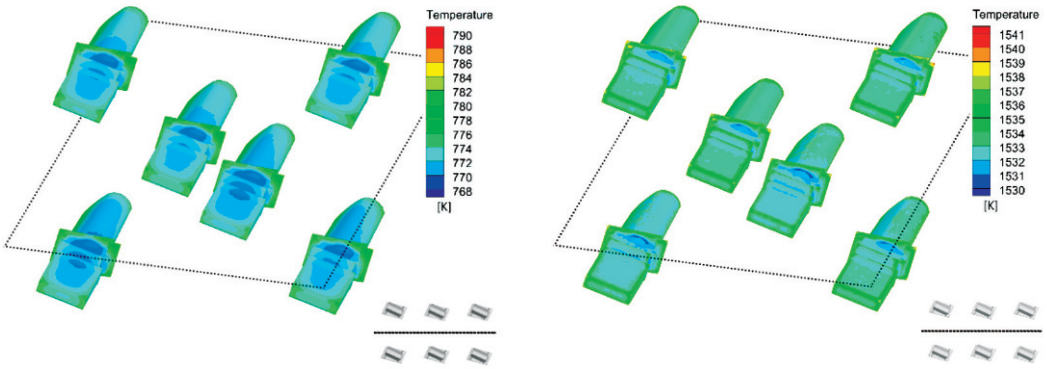

(a) heating, t = 3 h (b) holding, t = 8 h

Fig. 11: Temperature distribution of multiple blades with double layers during heating and holding stages

3.4 Flow field prediction during gas fan quenching process

The flow field has significant influences on the temperature distribution and the cooling rate of turbine blade during gas fan quenching continuous cooling process. Figure 12 presents the flow field prediction in the furnace, including the distribution on an axial cross section and two circular cross sections. Higher flow velocity is observed in the position close to the nozzles and the fan in section 1 and section 2 (Fig. 12). There are significant differences of flow field on circular cross section 2 and section 3, which is relevant to the axial distribution of nozzles. The complex structure of the practical vacuum chamber furnace has been considered, including the heating belt, the loading tray, and free outlet, which has different effects on the flow field, as illustrated in Fig. 13 and Fig. 14. Though the heating belts are close to the nozzle, the effect of gas flow is small (Fig. 13). The loading tray has strong disturbances to the flow field, and the high-speed gas flows out from the nozzle is divided by loading tray, resulting in the violent disturbance (Fig. 14). The free outlet enhanced the two vortex flow at the end of the furnace door. When a vortex exists at the end of the furnace door, the flow is strong at the places away from the fan and weak in the constant temperature zone (Fig. 14). For the quenched components, the flow is weak at the side facing the nozzle, but the flow is strong at the side close to the exhaust fan in the constant temperature zone.

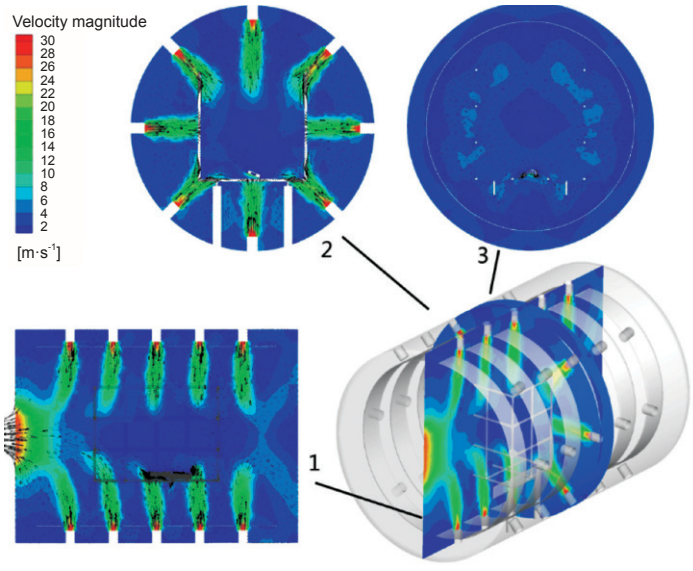

1– flow field distribution on an axial cross section,
2– on a circular cross section in which the nozzles are shown,
and 3– on a circular cross section which is between nozzles

Fig. 12: Simulation results of flow field distribution in furnace during gas fan quenching

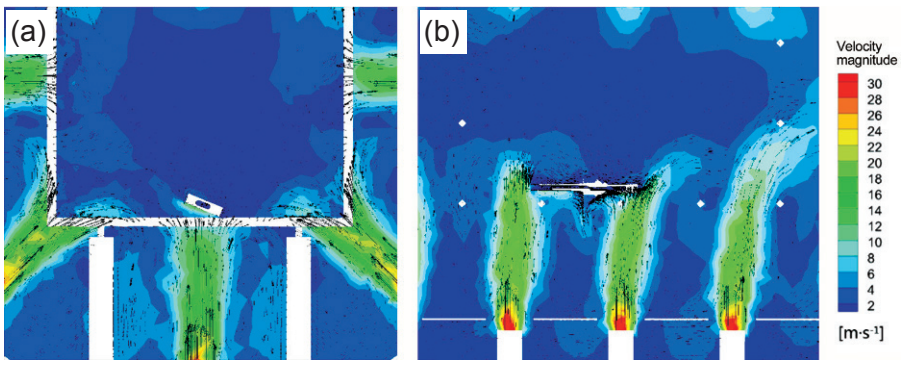

Fig. 13: Flow field in vicinity of loading tray (a) and heating belts (b)

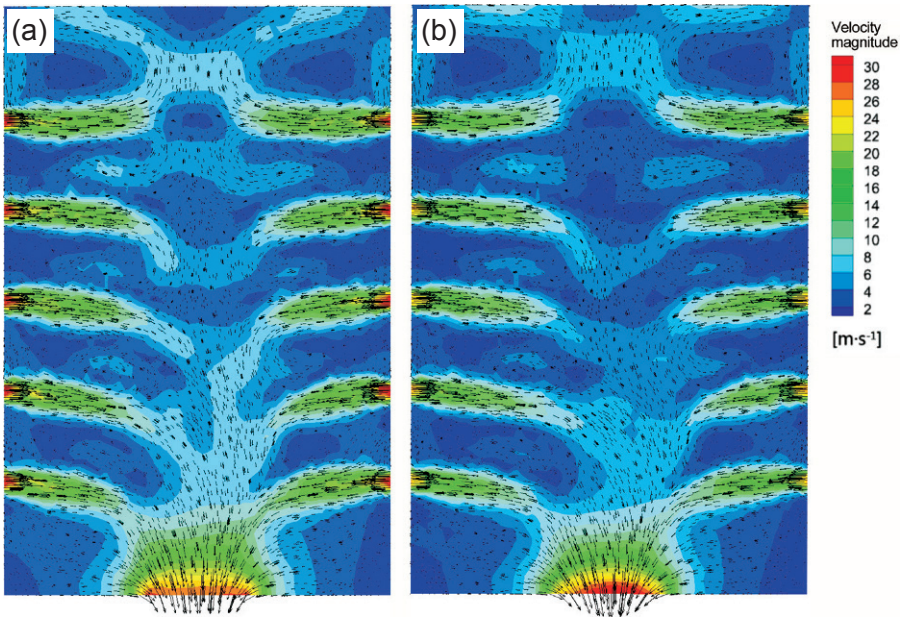

Fig. 14: Flow field with (a) and without a free outlet (b)

3.5 Temperature field prediction during gas fan quenching process

Figure 15 shows the cooling curves of an identical unit on blades surface under different pressures, indicating that the cooling rate is increased with the increase of the pressure. Figure 16 shows the change of temperature fields with time in the furnace under the pressure of 6 bar. The cooling rate of the loading tray is greater than that of the blade. It also can be seen that the circumferential cooling rate for the loading tray and blade is greater than that of the axial cooling rate. The local cooling rate for the loading tray changes obviously with the positions of the nozzle. The closer to the nozzle, the greater the cooling rate is.

Figure 17 demonstrates the temperature field evolution of a single blade during gas fan quenching. The complex structure of the blade itself leads to the non-uniform cooling, and the temperature of the unit at the thin-walled part is lower than that of the unit at the thick-walled part [Fig.17(a) and (b)]. The cooling temperature curves at different parts of the blade is presented in Fig. 17(e). The cooling rate at the sharp corner is greater than that at the tenon and blade platform. As shown in Fig. 17(c) and (d), the temperature at regions close to the internal position is decreased more slowly than that close to the surface.

3.6 Effect of number of turbine blades during gas fan quenching process

Figure 18 shows the flow filed distribution surrounding the multiple blades in one layer on a circular cross section. It indicates that the closer to the exhaust outlet and the nozzle for the blade, the greater the flow velocity is and the more the adequate flow is. Figure 19(a) and (b) shows the temperature distribution on surfaces of multiple blades in one layer at different time. Although the temperature at the sharp corner or thin wall in the blade that close to the nozzles is much lower, the temperature field distribution of blades in one layer is almost parallel [Fig. 19(a) and (b)]. Figure 19(c) and (d) presents the temperature distribution on the section of the blades. The cooling rate inside the air current channel is lower than that of at the position near the blade platform and tenon, and the effect of the blade location to the nozzles on the temperature field inside the blade is lower than that on the blade surface [Fig. 19(c) and (d)].

Simulation investigations are also conducted for multiple blades in double layers. The flow field around the multiple blades in double layers is shown in Fig. 20. It indicates that the flow velocity is low and the flow is not uniform for blades in the second-layer due to the shielding of the first-layer blade. Figure 21 shows the temperature distribution of multiple blades in two layers at different times. The cooling rate of the blades in the second-layer is obviously lower than that in the first-layer. The locating place has significant

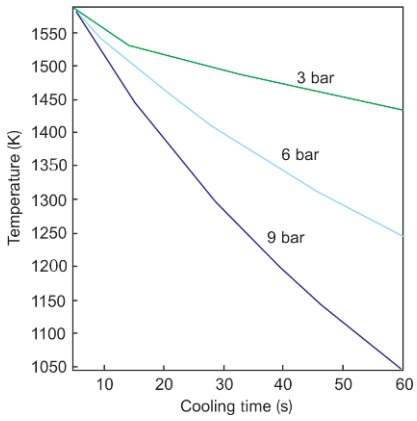

Fig. 15: Temperature in same point on surface of blade evolves as a function of time under various pressures during gas furnace quenching

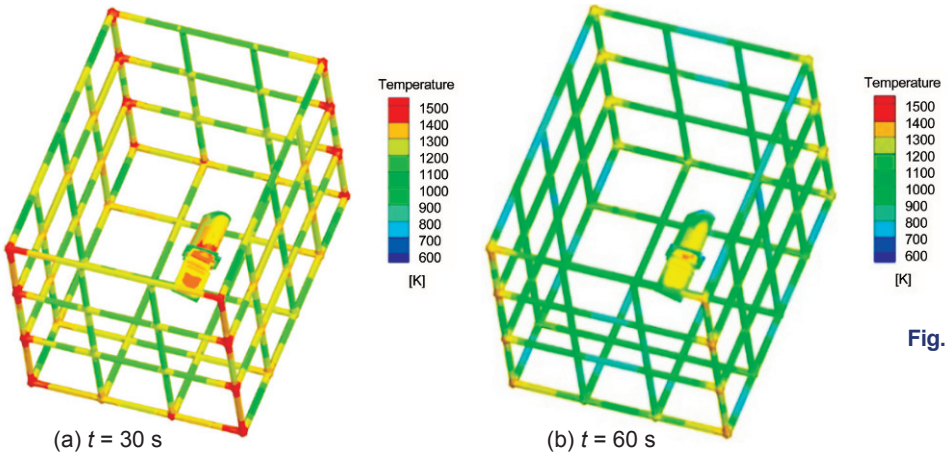

Fig. 16: Temperature distribution in furnace at different times during gas fan quenching under pressure of 6 bar

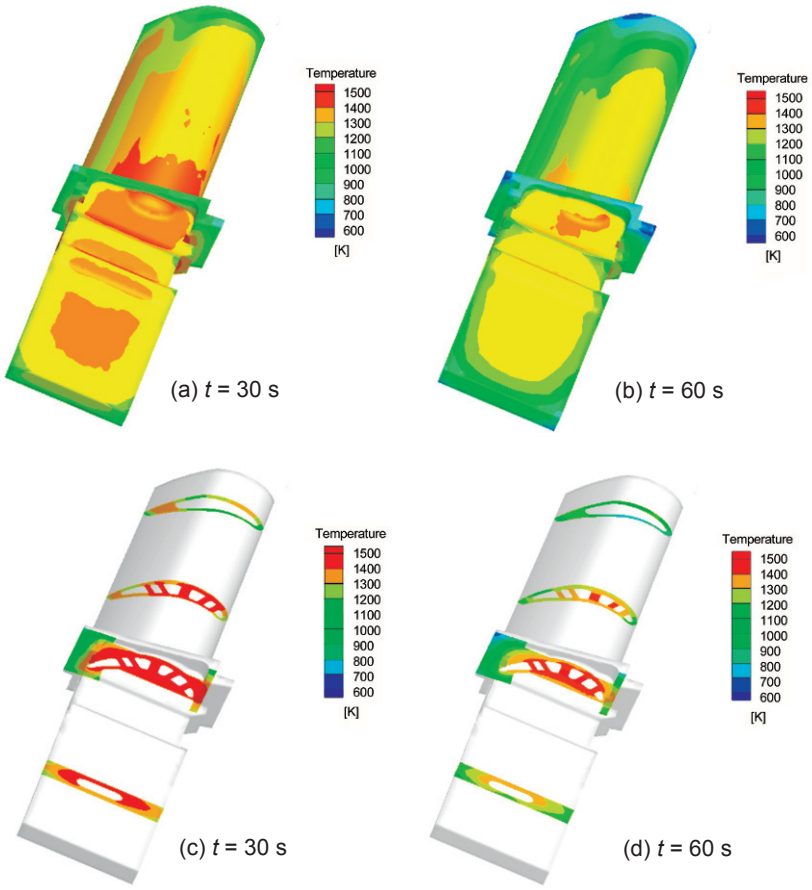

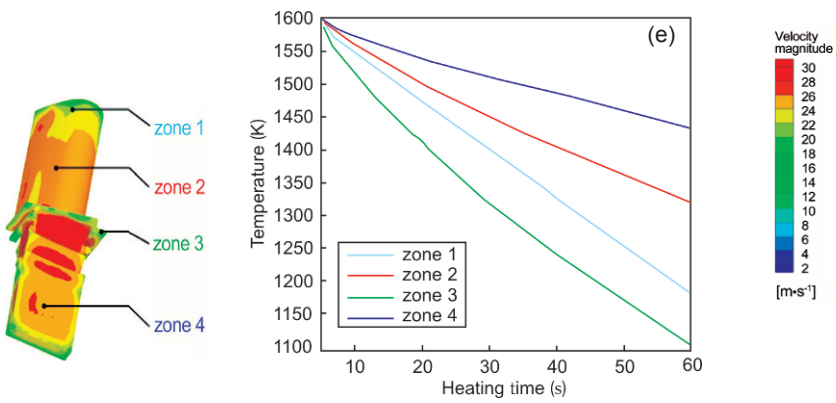

Fig. 17: Temperature distribution for a single blade at different times during gas fan quenching: (a) and (b) temperature profiles on blade surface, (c) and (d) temperature distribution in different sections of blade, and (e) temperature curves at different parts of blade

influences on the cooling rate of whole blade. The cooling rate of the blade close to the nozzles in the first-layer is higher than that of the blade away from the nozzles in the second-layer. Additionally, the temperature distribution on blades in the same layer is almost parallel, which is similar to the simulation results for the one layer. Figure 22 shows cooling temperature curves at different positions of the blade. It demonstrates that the blade structure has important effects on the local cooling rates for the blade in one layer. The cooling rate in the thin wall position of the blade away from the nozzles is larger than that in the tenon of the blade closer to the nozzles in the same layer. However, the cooling rate of the second-layer is much lower in both thin wall and tenon for the blades away from the nozzles in different layers.

From the numerical results presented above, the temperature field is affected by the heat treatment process and the number of turbine blades during the heating and solutionizing cooling. At the heating and holding stage, more attentions are paid to the uniformity of

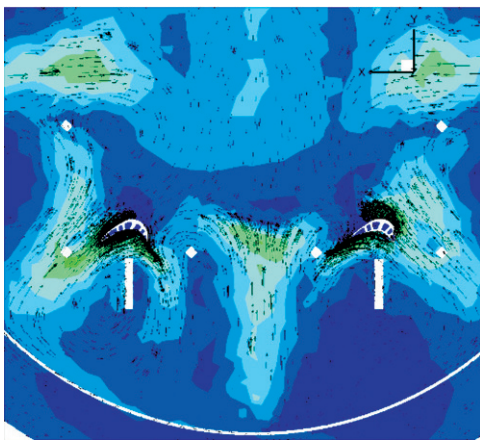

Fig. 18: Flow field surrounding multiple blades in one layer

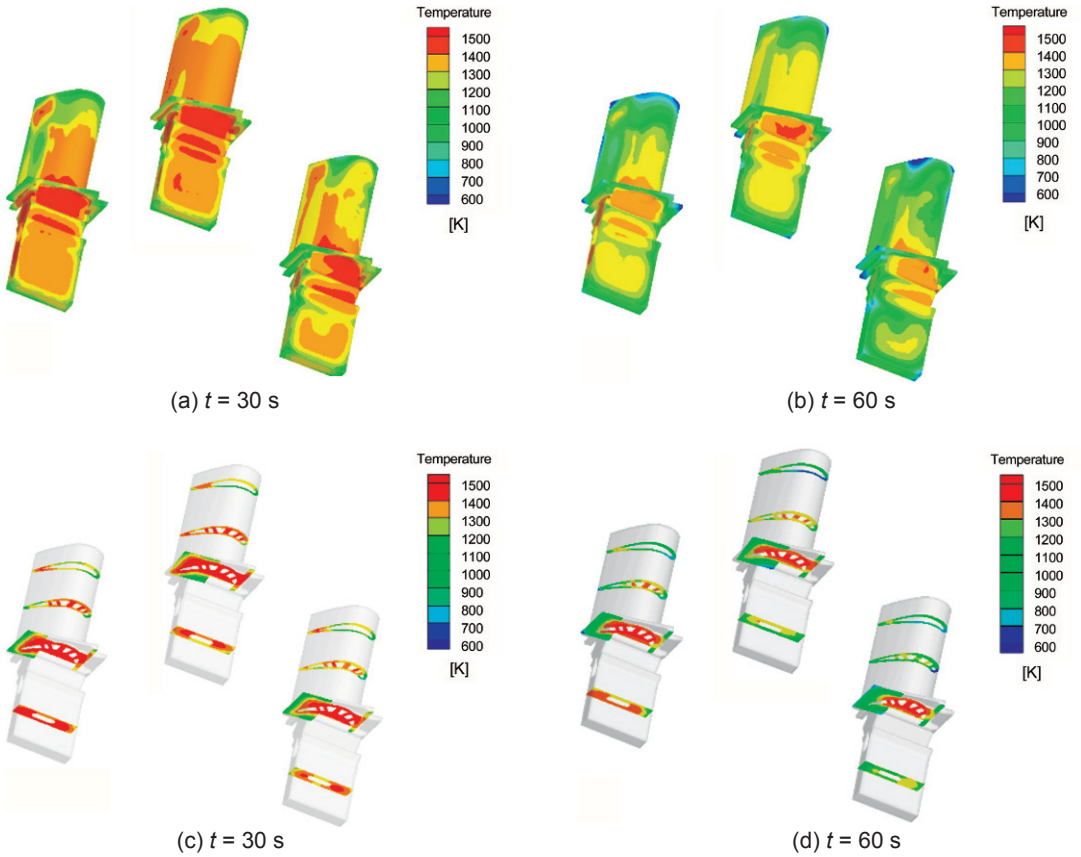

Fig. 19: Temperature distribution of multiple blades in one layer at different time: (a) and (b) temperature profiles on blade surface; (c) and (d) temperature distribution in different sections of turbine blade

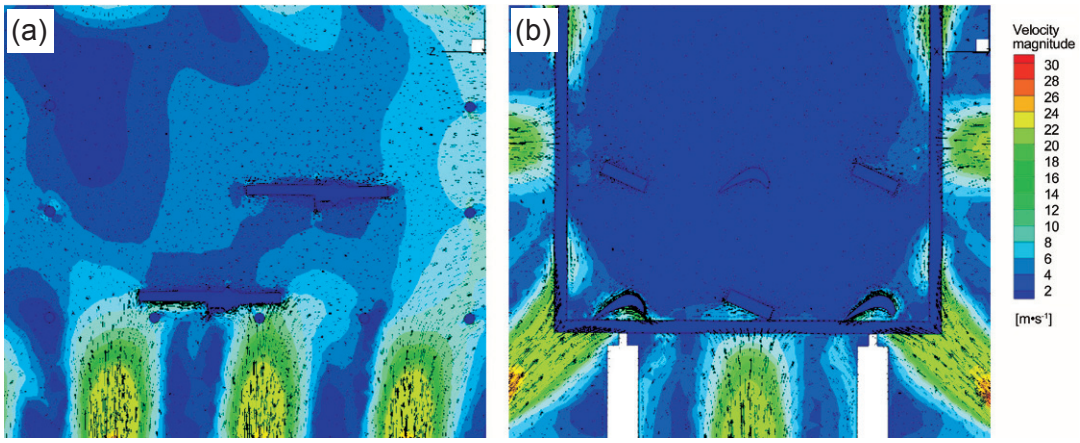

Fig. 20: Flow field around the multiple blades in double layers

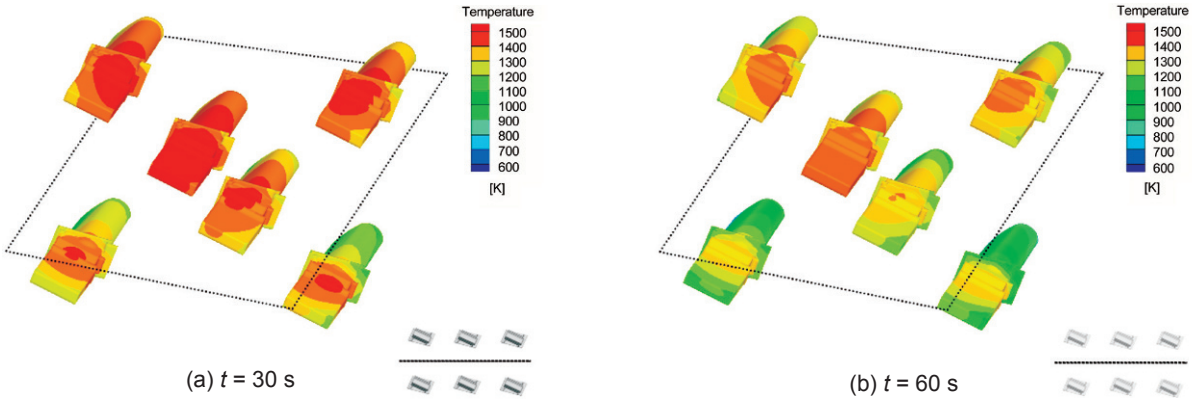

Fig. 21: Temperature distribution of multiple blades in two layers

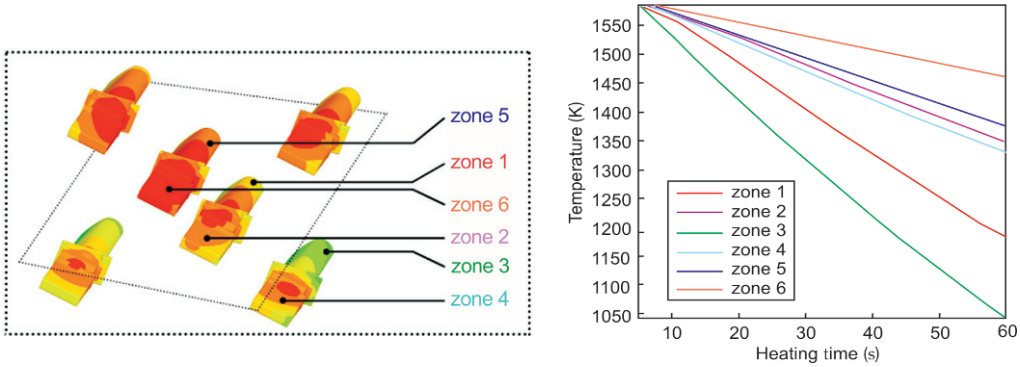

Fig. 22: Temperature curves of different zones in turbine blades

the temperature field for the blades in furnace. During gas fan quenching, more attention is paid to the manipulation of the cooling rate. There are some similarities for the influence of number of turbine blades during the gas quenching process with that during the heating and cooling process. The temperature change of the thick-walled part is slower than that of the thin-walled part. The temperature uniformity of a single layer turbine blade during heating and cooling can be controlled by the requirement of the heat treatment for the multiple components. However, the cooling rate is difficult to meet the requirement for turbine blades in two and more layers.

4 Conclusions

The numerical heat-transfer and turbulent flow model are established tomodel the heating, holding and gas fan quenching process of a low rhenium-bearing Ni-based single crystal turbine blades based on the CFD software and the practical chamber 3D-reconstruction of an industrial high-pressure quenching vacuum heat-treatment furnace. The following conclusions can be concluded:

(1) In load-free heating process, simulation result with UDF power input boundary condition is approached to the experiment results. Simulation results demonstrate that the turbine blade geometry, the shielding of the blade its own and the shielding among blades has significant influences on uniformity of the temperature distributions. The temperature distribution at the sharp corner, thin wall and corner part is higher than that at the thick wall part of turbine blade during heating process, and the isotherms show a toroidal line to the center of the thick wall. The temperature uniformity during holding stage is better than that during heating stage. The temperature of sheltered units is lower than that of the remaining part of turbine blade. When there is no shelteration among multiple blades, the temperature distribution for all turbine blades is almost identical, and the temperature difference among the blades is smaller than the difference for the blade itself.

(2) The loading tray, free outlet and the place of turbine blades have important influences on the flow field. The high-speed gas flows out from the nozzle is divided by loading tray, and the free outlet enhanced the two vortex flow at the end of the furnace door. The turbine blade is closer to the exhaust outlet and the nozzle, the flow velocity is greater and the flow is more adequate.

(3) The cooling rates are enhanced with the increase of the pressure, and the complex structure of the turbine blade plays a crucial role in the temperature distribution for a single blade during gas fan quenching. The cooing rate at the thin-walled part is lower than that at the thick-walled part, the cooling rate at the sharp corner is greater than that at the tenon and blade platform, and the temperature at regions close to the internal position is decreased more slowly than that close to the surface.

(4) The locating place and the complex structure of the components have significant impacts on the cooling rates. However, the effects of complex structure of turbine blades in double layers differs from that in single layer.

(5) The effects of complex structure of turbine blades in double layers differs form that in single layer. For multiple blades in single layer, the temperature at the sharp corner or thin wall in the blade that close to the nozzles is much lower, the temperature field distribution of blades is almost parallel. The cooling rate inside the air current channel is lower than that of at the position near the blade platform and tenon, and the effect of the blade location to the nozzles on the temperature field inside the blade is lower than that on the blade surface. For multiple blades in double layers, the flow velocity is low, and the flow is not uniform for blades in the second-layer due to the shielding of the first-layer blade. The cooling rate of the blades in the second-layer is lower than that in the first-layer, the cooling rate of the blade close to the nozzles in the first-layer is the higher than that of the blade away from the nozzles in the second-layer, the temperature distribution on blades in the same layer is almost parallel, which is similar to the simulation results for the first layer. The cooling rate in the thin wall position of the blade away from the nozzles is larger than that in the tenon of the blade closer to the nozzles in the same layer. The cooling rate of the second-layer is much lower in both thin wall and tenon for the blades away from the nozzles in different layers.

References

[1] Daniel G B, James C W. Advanced materials for aircraft engine applications. Science, 1992, 255(5048): 1082–1087.
[2] Fei Sun, Jinyan Tong, Qiang Feng, et al. Microstructural evolution and deformation features in gas turbine blades operated in-service. Journal of Alloys and Compounds, 2015, 618: 728–733.
[3] Roger C R. The superalloys fundamental and applications. Cambridge, Cambridge University Press, 2006.

[4] Jayaram R, Miller K M. Influence of phase composition and microstructure on the high temperature creep properties of a model single crystal nickel-base superalloy: An atom probe/AEM study. Acta Metallurgica et Materialia, 1995, 43(05): 1979–1986.
[5] Sammy T, Tresa M P. Nickel-based superalloys for blade application: production, performance and application. Encyclopedia of Aerospace Engineering, 2010, 1–13. DOI: 10.1002/9780470686652.eae218.
[6] Pierre C, Tasadduq K. Evolution of Ni-based superalloys for single crystal gas turbine blade applications. Aerospace Science and Technology, 1999, 3: 513–23.
[7] Walston S, Cetel A, MacKay R, et al. Joint development of a fourth generation single crystal superalloy. Proc. 10th. Int. Symp. On Superalloys 2004, Champion, PA, USA, September 2004, TMS, 15–24.
[8] Zhang Jianxin, Murakumo T, Koizumi Y, et al. The influence of interfacial dislocation arrangements in a fourth generation single crystal TMS-138 superalloy on creep properties. Journal of Materials Science, 2003, 38: 4883–4888.
[9] Akihiro S, Hiroshi H, An C Y, et al. A 5th generation SC superalloy with balanced high temperature properties and processability. Proc. 8th. Int. Symp. On Superalloys 20008, Champion, PA, USA, September 2008, TMS, 131–138.
[10] Kyoko K, An C Y, Tadaharu Y, et al. Development of an oxidation-resistant high-strength six-generation single-crystal superalloy. Proc. 12th. Int. Symp. On Superalloys 2012, Champion, PA, USA, September 2012, TMS, 189–195.
[11] Yuan Y, Kawagishi K, Koizumi Y, et al. Creep deformation of a sixth generation Ni-base single crystal superalloy at 800ºC. Materials Science & Engineering A, 2014, 608: 95–100.
[12] Dai Huijuan. A Study of solidification structure evolution during investment casting of Ni-based superalloy for aero-engine turbine blades. Ph.D. thesis, Department of Engineering, University of Leicester, 2008.
[13] Pan Dong; Xu Qingyan; Liu Baicheng; et al. Modeling of Grain Selection during Directional Solidification of Single Crystal Superalloy Turbine Blade Castings. JOM, 2010, 62(5): 30–34
[14] Kearney R M, Beddoes J C, Jones P, et al. Compositional design considerations for microsegregation in single crystal superalloy systems. Intermetallics, 2004, 12: 903–910.
[15] Pang Hontong, Laguna Zhang, Robbie A. Hobbs, et al. Solution heat treatment optimization of fourth-generation Single-Crystal nickel-base superalloys. Metallurgical and Materials Transaction A, 2012, 43(09): 3264–3282.
[16] Pang Hontong, Neil D S, Dong Hongbiao, et al. Detailed analysis of the solution heat treatment of a third-generation single-crystal nickel-based superalloy CMSX-10K. Metallurgical and Materials Transaction A, 2016, 47(02): 889–906.
[17] Fuchs G E. Solution heat treatment response of a third generation single crystal Ni-base superalloy. Materials Science and Engineering A, 2001, 300: 52–60.
[18] [18] Hegde S R, et al. Design of solutionizing heat treatments for an experimental single crystal superalloy. Proc. 11th. Int. Symp. On Superalloys 2008, Champion, PA, USA, September 2008, TMS, 301–310.
[19] Hedge S R, Kearsey R M, Beddoes J C. Designing homogenization-solution heat treatments for single crystal superalloys. Materials Science and Engineering A, 2010, 527: 5528–5538.
[20] Ma Wenyou, Li Shusuo, Qiao Min, et al. Effect of heat treatment on microstructure and high temperature stress rupture properties of nickel-based single crysatal superalloy. The Chinese Journal of Nonferrous Metals, 2006, 16(06): 937–944. (In Chinese).
[21] Fuchs G E, Boutwell B A. Modeling of the partitioning and phase transformation temperatures of an as-cast third generation single crystal Ni-base superalloy. Materials Science and Engineering A, 2002, 333: 72–79.
[22] Pai B R, Michelfelder S, Spalding D B. Prediction of furnace heat transfer with a three-dimensional mathematical model. International Journal of Heat and Mass Transfer, 1978, 21(5): 571–580.
[23] Kang Jinwu, Rong Yiming. Modeling and simulation of load heating in heat treatment furnaces. Journal of Materials Processing Technology, 2006, 174(1): 109–114.
[24] Li Huiping, Zhao Guoqun, Huang Chuanzhen, et al. Technological parameters evaluation of gas quenching based on the finite element method. Computational Materials Science, 2007, 40(2): 282–291.
[25] Elkatatny I, Morsi Y, Blicblau A S, et al. Numerical analysis and experimental validation of high pressure gas quenching. International Journal of Thermal Sciences, 2003, 42: 417–423.
[26] Wang Jing, Gu Jianfeng, Shan Xuexiong, et al. Numerical simulation of high pressure gas quenching of H13 steel. Journal of Materials Processing Technology, 2008, 202(1): 188–194.
[27] Francesco C, Nils W, Jean C G, et al. Numerical Modeling of Vacuum Heat Treatment of Nickel-based Superalloys. Metallurgical and Materials Transactions A, 2013, 44(11): 5154–5164.
[28] Francesco C, Nils W, Jean C G, et al. Numerical and experimental study of post-heat treatment gas quenching and its impact on microstructure and creep in CMSX-10 superalloy. Journal of Materials Processing Technology, 2013, 213: 2350–2360.
[29] Francesco C, Nils W, Jean C G, et al. Multi-scale modeling of high pressure gas fan quenching for gas turbine applications. In: Proc. Ninth International Conference on CFD in the Minerals and Process Industries CSIRO, Melbourne, Australia, 2012: 1–6.
[30] Li Jiarong, Zhong Zhenggang. Tang Dingzhong, et al. A low cost second generation single crystal superalloy DD6. Proc. 9th. Int. Symp. On Superalloys 2000, Champion, PA, USA, September 2000, TMS, 777–783.
[31] Pierre C, Tasadduq K. Evolution of Ni-based superalloys for single crystal gas turbine blade applications. Aerospace Science Technology, 1999, 3: 513–523.
[32] Macchion O. CFD in the design of gas quenching furnace. Technical Reports, Department of Mechanics, Royal Institute of Technology, 2005.
[33] Wang Zhijian, Shang xiaofeng, Flow and Heat-Transfer Simulation Based on CFD and Experimental Study during High-Pressure Gas Quenching. Applied Mechanics and Materials, 2010, 29: 1436–1440.
[34] The editorial board for handbook of engineering materials. Handbook of engineering materials (2nd edition). Beijing, China Standard Press, 2002: 771. (In Chinese)

This research was financially supported by the National Natural Science Foundation of China (grant nos. 51374137 and 51171089), National Science and Technology Major Special Project of China (grant no.2012ZX04012-011), and National Basic Research Program of China (grant no. 2011CB706801).